The Astronomical Journal, 172:287 (12pp), 2026 November https://doi.org/10.3847/1538-3881/aeaee4
© 2026. The Author(s). Published by the American Astronomical Society.
OPEN ACCESS

Discovery and Characterization of the TOI-4468 Planetary System: A Transiting Hot Jupiter with a Lone Nearby Outer Companion

Joseph R. Livesey[1], Benjamin J. Hord[2], Juliette Becker[1], Andrew Vanderburg[3], Joseph E. Rodriguez[4], Elise Koo[5,6], Chelsea X. Huang[7], Guðmundur Stefánsson[5,8], Karen A. Collins[3], Ivan A. Strakhov[9], Zijun He[10], Maxwell A. Kroft[1], Robert Aloisi[1], Khalid Barkaoui[11,12,13], Fabian Rodriguez Frustaglia[14], Alyssa Jankowski[1], Kinga Kasprzyk[15], Judith Korth[16], Coleman Nelson[1], Hannu Parviainen[11,17], Adam Popowicz[15], Manfred Raetz[18], Richard P. Schwarz[3], Eva Stafne[1], Keivan G. Stassun[19], Thomas G. Beatty[1], Paul Foster[20], Thomas MacLean[21,22], Devansh Mathur[1], Lizhou Sha[1,23], and Melinda Soares-Furtado[1]

[1] Department of Astronomy, University of Wisconsin–Madison, Madison, WI 53706, USA; jrlivesey@wisc.edu
[2] NASA Goddard Space Flight Center, Greenbelt, MD 20771, USA
[3] Center for Astrophysics | Harvard & Smithsonian, Cambridge, MA 02138, USA
[4] Center for Data Intensive and Time Domain Astronomy, Department of Physics and Astronomy, Michigan State University, East Lansing, MI 48824, USA
[5] Anton Pannekoek Institute for Astronomy, University of Amsterdam, Amsterdam XH 1098, The Netherlands
[6] ASTRON, Netherlands Institute for Radio Astronomy, Dwingeloo 7991 PD, The Netherlands
[7] Centre for Astrophysics, University of Southern Queensland, Toowoomba, QLD 4350, Australia
[8] Astrophysics & Space Institute, Schmidt Sciences, New York, NY 10011, USA
[9] Sternberg Astronomical Institute, Lomonosov Moscow State University, Moscow 119992, Russia
[10] Madison West High School, Madison, WI 53726, USA
[11] Instituto de Astrofísica de Canarias (IAC), La Laguna 38200, Tenerife, Spain
[12] Astrobiology Research Unit, Université de Liège, Liège 4000, Belgium
[13] Department of Earth, Atmospheric and Planetary Science, Massachusetts Institute of Technology, Cambridge, MA 02139, USA
[14] Frustaglia Private Observatory, Spain
[15] Silesian University of Technology Observatory, Gliwice, Poland
[16] Lund Observatory, Division of Astrophysics, Department of Physics, Lund University, Lund 22100, Sweden
[17] Departamento de Astrofísica, Universidad de La Laguna (ULL), La Laguna, Tenerife, Spain
[18] Privat Observatory Herges-Hallenberg, Steinbach-Hallenberg, Germany
[19] Department of Physics & Astronomy, Vanderbilt University, Nashville, TN 37235, USA
[20] California State University, Los Angeles, Los Angeles, CA 90032, USA
[21] California Institute of Technology, Pasadena, CA 91125, USA
[22] Department of Aeronautics and Astronautics, Stanford University, Stanford, CA 94305, USA
[23] Department of Astrophysical Sciences, Princeton University, Princeton, NJ 08544, USA
Received 2026 May 4; revised 2026 August 7; accepted 2026 August 25; published 2026 October 29

Abstract

We report the discovery of two planets, a hot Jupiter (HJ) and a nearby outer sub-Neptune, orbiting the star TOI-4468. This system is unique among the current exoplanet census in that it features a close outer companion to a HJ without an accompanying inner companion. By jointly fitting radial velocity (RV) measurements taken with the NEID spectrograph and transit photometry from the Transiting Exoplanet Survey Satellite (TESS) and several ground-based observatories, we constrain the orbital periods, masses, and radii of these two planets. We confirm the planetary nature of the HJ TOI-4468 b ($R = 1.01R_J$, $m = 0.54M_J$, $P = 2.77$ days). We also validate the outer planet TOI-4468 c ($R = 0.28R_J$, $P = 7.01$ days) statistically, incorporating constraints from ground-based observations. We also identify, but cannot confirm, an additional RV signal that may be due to an outer giant in this system with an orbital period of 624 days. From the observed geometry of this system, we argue that it must never have encountered an early secular resonance that is thought to excite the mutual inclination of other HJ/outer companion systems. We discuss the possibility of an undetected inner companion, as well as potential implications for HJ formation.

Unified Astronomy Thesaurus concepts: Exoplanet astronomy (486); Exoplanet dynamics (490); Radial velocity (1332); Hot Jupiters (753); Transit photometry (1709)

1. Introduction

Constraining the formation mechanisms that produce hot Jupiters (HJs)—which, due to their ease of detection, are among the most abundant classes of exoplanets in the present observational sample despite being intrinsically rare (M. Beleznay & M. Kunimoto 2022)—has been an ongoing effort in exoplanet astronomy since the discovery of the first specimen, 51 Pegasi b (M. Mayor & D. Queloz 1995). Among the plausible formation channels are (i) in situ formation, (ii) disk-driven migration, and (iii) high-eccentricity migration, driven either by a stellar flyby or planet–planet scattering in the outer system (R. Dawson & J. A. Johnson 2018). Channel (i) requires a large surface density of refractory material at the inner edge of the initial protoplanetary disk, which can possibly be supplied in the presence of multiple short-period super-Earths (K. Batygin et al. 2016; A. C. Boley et al. 2016). A principal line of evidence favoring channel (iii) is that HJs tend to have outer giant companions, and these companions exhibit the same distribution of orbital periods as those in

Original content from this work may be used under the terms of the Creative Commons Attribution 4.0 licence. Any further distribution of this work must maintain attribution to the author(s) and the title of the work, journal citation and DOI.

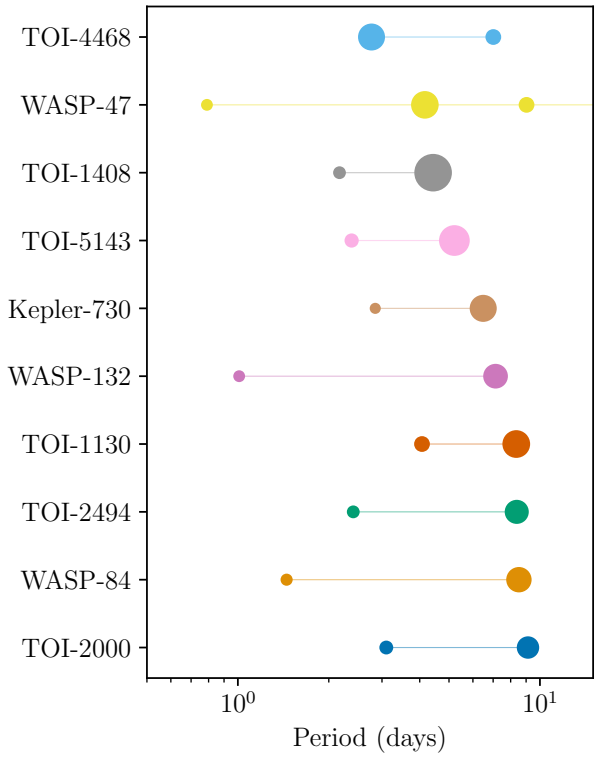


Figure 1. Known HJ systems containing nearby companions, with planetary radii to scale. WASP-47 b bears both an outer companion and an inner ultra-short-period planet, along with the cold giant WASP-47 c at 590 days. TOI-4468 is the first known system containing only a HJ and a nearby outer companion. The other eight systems exhibit only nearby inner companions.

warm and cold Jupiter systems (J. K. Zink & A. W. Howard 2023). Thus, HJs are connected to their outer systems, and do not typically comigrate with their companions, as expected for disk-driven migration.

Channel (iii) likely precludes the existence of nearby exterior companions, as these planets would be driven unstable by dynamical interactions with the migrating HJ (A. J. Mustill et al. 2015), and also precludes the existence of inner companions, as even ultra-short-period companions that might appear dynamically detached will not survive the migration process (J. Becker 2026). Several HJs have previously been discovered to have small inner companions. Almost all of these systems comprise solely the HJ and the inner companion, e.g., TOI-1130 (C. X. Huang et al. 2020), TOI-2000 (L. Sha et al. 2023), TOI-1408 (J. Korth et al. 2024), TOI-5143 (B. T. Radzom et al. 2025; S. N. Quinn et al. 2026), TOI-2494 (S. N. Quinn et al. 2026), Kepler-730 (C. I. Cañas et al. 2019), and WASP-132 (B. J. Hord et al. 2022). WASP-47 is the only HJ system containing a nearby outer companion in addition to the inner (J. C. Becker et al. 2015). These HJs could not have formed through channel (iii), and thus either formed in situ or migrated inward due to disk torques.

A recent analysis by L. Sha et al. (2026) determined a mean occurrence rate of 7.6% for nearby companions to HJs. The census of HJs with nearby companions is presented in Figure 1. The lack of observed nearby outer companions to HJs has been attributed to secular interactions between the two planets and the host star. In particular, as a low-mass star (below the Kraft break) loses angular momentum to its wind, it becomes less oblate as a consequence. The quadrupole moment of its gravitational field—parameterized by J_2, the leading-order zonal harmonic—decreases as a result. Consequently, the quadrupolar contribution to the planets' secular frequencies weakens, and when a critical value of J_2 is reached, a resonance between the secular frequencies and the instantaneous nodal regression rates of the planets is swept, amplifying their mutual inclination (C. Spalding & K. Batygin 2016, 2017; T. MacLean & J. Becker 2025). The expectation that this resonance—which acts only on two-planet systems in which the inner planet harbors significantly more angular momentum than the outer—affects the majority of HJ/outer companion systems explains the lack of such architectures in the observational census. Because the mutual inclination has been amplified in such a system, we will not see the companion transit if we see the HJ.

In this work, we present the discovery and dynamical characterization of the TOI-4468 (TIC 441763252) system. This system centers on a $T_{\rm eff} = 5200$ K K dwarf and is the second observed, after WASP-47, that contains a HJ and a nearby outer companion, and is the first observed with *only* an outer companion. This novel architecture presents the opportunity to further investigate the formation mechanism of HJs with nearby companions. In Section 2, we explain the data used in our characterization of the system, including radial velocity (RV) measurements and transit photometry from multiple sources. We describe our analysis of the fitted data, the confirmation of the HJ, and statistical validation of the companion in Section 3. We discuss these results and consider the possibility of an additional inner companion in Section 4, and conclude in Section 5.

2. Data

2.1. TESS Photometry

TOI-4468 was observed by the Transiting Exoplanet Survey Satellite (TESS). TESS observes stars in periods of time known as sectors, each lasting about 28 days, where the spacecraft maintains stable pointing at one part of the sky. Some regions of the sky, known as the "continuous viewing zone," are observed nearly continuously even as TESS's pointing moves from sector to sector. TOI-4468 falls near the continuous viewing zone, and as a result has been observed frequently over the course of the TESS mission. TOI-4468 has been observed by TESS for a total of 39 sectors as of November 2025. For the first year of observations (the second year of the TESS mission, Sectors 14–26), TOI-4468 was not preselected for fast-cadence observations, and instead was observed in the TESS Full Frame Images, which were at that time coadded to 30 minute exposures. It was identified as a planet candidate host star by G. Olmschenk et al. (2021) and was then selected for faster (2 minute) cadence observations in all sectors thereafter. After a considerable number of 2 minute light curves were collected, a second planet candidate was identified and released by the TESS mission.

We reduced the data from the Full Frame Images following A. Vanderburg et al. (2019); in short, we extracted photometry from 20 different photometric apertures, corrected for systematics by decorrelating moments of the spacecraft quaternion time series and the background flux outside the aperture, and corrected for blending from outside the aperture. We used the standard TESS Science Processing and Operations Center (SPOC; J. M. Jenkins et al. 2016) light curves for the 2 minute cadence observations. We flattened both the 30 minute cadence

Full Frame and 2 minute cadence light curves following J. Pepper et al. (2020) and used these light curves in our global modeling. Our Full Frame Images were taken in Sectors 14–26, and 2 minute cadence data from Sectors 41, 48–60, 73, and 75–80.

2.2. Ground-based Photometry

The TESS pixel scale is $\sim 21''$ pixel^{-1}, and photometric apertures typically extend out to roughly $1'$, generally causing multiple stars to blend in the TESS photometric aperture. To determine the true source of the TESS detections, we acquired ground-based time-series follow-up photometry of the field around TOI-4468 as part of the TESS Follow-up Observing Program Sub Group 1 (TFOP SG1; K. Collins 2019).[24] We used the TESS Transit Finder, which is a customized version of the TAPIR software package (E. Jensen 2013), to schedule our transit observations.

We used ASTROIMAGEJ (K. A. Collins et al. 2017) to extract differential photometric data from five TOI-4468 b image sequences and one TOI-4468 c image sequence, as detailed below. The light-curve data were extracted using circular photometric apertures having radii ranging from $5\farcs2$ to $10\farcs1$. The target-star apertures excluded all flux from all known Gaia DR3 catalog neighbors. Transit-like signals were detected in the target-star apertures in all six light curves, confirming that both TESS-detected transit-like events indeed originate from TOI-4468. The light-curve data are available on the ExoFOP-TESS website.[25] The light curves are included in the global model described in Section 3.1 and are shown in Figure 4.

2.2.1. Herges-Hallenberg 0.28 m

We observed a transit egress window of TOI-4468 b with no filter on UTC 2022 March 18 from the Privat Observatory Herges-Hallenberg 0.28 m telescope near Steinbach-Hallenberg, Germany. The telescope is equipped with a Moravian Instrument G2-1600 detector with an image scale of $1\farcs02$ pixel^{-1}, resulting in a $27' \times 41'$ field of view. Images were calibrated using ASTROIMAGEJ.

2.2.2. Frustaglia Observatory 0.3 m

We observed three full transit windows of TOI-4468 b on UTC 2023 January 11, 2023 April 7, and 2025 December 17 from the Frustaglia Private Observatory 0.3 m telescope located near Fregenal de la Sierra, Spain (RFAC). The telescope is equipped with a 6248 × 4176 QHY 268M camera having an image scale of $0\farcs32$ per pixel, resulting in a $33' \times 22'$ field of view. The images were calibrated using ASTROIMAGEJ.

2.2.3. Las Cumbres Observatory Global Telescope 1.0 m

We observed a full transit window of TOI-4468 c on UTC 2024 August 16 and a full transit window of TOI-4468 b on UTC 2025 April 25, both in the Sloan i' band, from the Las Cumbres Observatory Global Telescope (LCOGT; T. M. Brown et al. 2013) 1.0 m network node at Teide Observatory on the island of Tenerife. The 1 m telescopes are equipped with 4096 × 4096 SINISTRO cameras having an image scale of $0\farcs389$pixel^{-1}, resulting in $26' \times 26'$ field of views. The images were calibrated by the standard LCOGT BANZAI pipeline (C. McCully et al. 2018).

2.2.4. Silesian University of Technology Observatory

We observed a full transit on UT 2022 March 9 from the Silesian University of Technology Observatory (SUTO) 0.3 m telescope located near Otivar, Spain. The telescope is equipped with a 4656 × 3520 pixel ASI ZWO 1600MM camera. The image scale is $0\farcs685$ pixel^{-1}, resulting in a $53' \times 42'$ field of view. The photometric data were extracted with ASTROIMAGEJ using a circular $7\farcs2$ aperture.

Table 1
Radial Velocities Measured with NEID

Epoch (BJD_{TDB})	Radial Velocity (m s^{-1})	Error (m s^{-1})
2460194.68192	6.2	7.4
2460236.66439	−82.9	9.7
2460239.59063	−101.96	8.7
2460327.99483	−58.0	6.3
2460329.00208	−107	11
2460341.94347	−69	10
2460411.96062	−99.8	8.1
2460447.70677	−98	10
2460454.76181	84.7	7.5
2460472.83070	−87.5	6.2
2460595.62048	58.7	7.1
2460753.93099	63.4	5.8
2460755.92351	−46.6	6.2

2.3. Radial Velocities

Our RV measurements were taken with NEID, an ultraprecise, stabilized (G. Stefánsson et al. 2016; P. Robertson et al. 2019), fiber-fed (S. Kanodia et al. 2023) spectrograph on the WIYN 3.5 m Telescope. NEID has continuous broadband wavelength coverage between 380 and 930 nm. Our observations used the high-efficiency mode, with a spectral resolving power of $R = 60{,}000$. We have 13 total data points each with an exposure time of roughly 3300 s, which were taken between summer 2023 and spring 2025. The individual measurements are given in Table 1.

The RVs were extracted with the spectral-matching method, using a code inspired by the SpEctrum Radial Velocity AnaLyzer (SERVAL; M. Zechmeister et al. 2018) but adapted for NEID (G. Stefánsson et al. 2022). As this pipeline is optimized for faint targets it is useful for TOI-4468, which has an apparent V-band magnitude of 14.2. These extracted SERVAL RVs agree well with the cross-correlation function (CCF) RVs extracted through the standard NEID pipeline, while reducing the median error from 91.49 to 8.11 m s^{-1}. Our observations have signal-to-noise ratios ranging between 10 and 18, and were taken at air masses between 1.32 and 1.95.

2.4. Stellar Spectral Energy Distribution

We adopt the spectral energy distribution (SED) values reported in ExoFOP for TOI-4468 as our priors, as listed in Table 2. These values were derived in the TESS Input Catalog (TIC) following the methods described in K. G. Stassun et al. (2018). The output SED from our EXOFASTV2 global fit of the system (Section 3.1) is shown in Figure 2(a).

[24] https://tess.mit.edu/followup
[25] https://exofop.ipac.caltech.edu/tess/target.php?id=441763252

Table 2
Spectral Energy Distribution of TOI-4468 in Magnitudes

Band	Magnitude	Error (mag)
B	14.86	0.12
V	14.08	0.20
Gaia *G*	13.8677	0.0004
g'	15.1888	0.0039
r'	13.9853	0.0026
i'	14.2862	0.0053
z'	13.7478	0.0047
2MASS *J*	12.453	0.020
2MASS *H*	11.977	0.019
2MASS *K*	11.890	0.024
WISE 3.4 μm	11.873	0.022
WISE 4.6 μm	11.936	0.021
WISE 12 μm	11.97	0.17

2.5. Speckle Imaging

We observed TOI-4468 on 2024 February 28 using speckle interferometry with the Speckle Polarimeter (SPP), a facility instrument on the 2.5 m telescope at the Caucasian Observatory of the Sternberg Astronomical Institute (SAI) of Lomonosov Moscow State University (I. A. Strakhov et al. 2023). We used a fast, low-noise Hamamatsu ORCA-Quest CMOS camera as a detector and an I_c filter. The pixel scale was 20.6 mas pixel^{-1}. The power spectrum was estimated from 2500 frames per star, each with 60 ms exposure time, and is shown in Figure 2(b). The atmospheric dispersion compensator was employed. We did not detect a stellar companion. The detection limits are 3.1 mag and 4.2 mag at 0.″25 and 1.″0 from the star, respectively.

3. Analysis

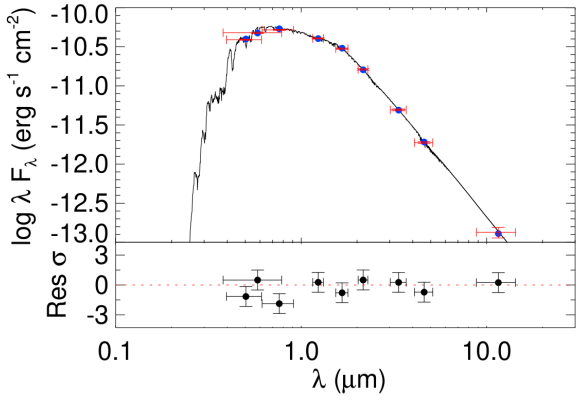
3.1. Global System Characterization

We use the EXOFASTV2 code (J. D. Eastman et al. 2019) to self-consistently model the star and both planets in the TOI-4468 system, constraining the planetary properties by jointly fitting transit data from TESS, RFAC, LCOGT, and SUTO and RVs measured with the NEID spectrograph. The TESS data comprise 311 transits of planet b in total, including eight partial transits. We do not fit RVs for planet c, as its signal is below the noise threshold for NEID (3.85 m s^{-1} for a mass of $10M_\oplus$). Aside from an uninformative uniform prior for the dust extinction, our priors are taken from Gaia. They are listed in Table 3.

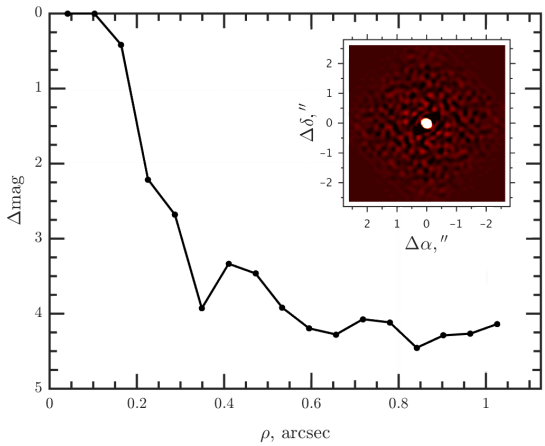
We verify the convergence of our EXOFASTV2 fit by running it until the Gelman–Rubin statistic (A. Gelman & D. B. Rubin 1992) falls below 1.01 (see, e.g., J. D. Eastman et al. 2019). We find mean planetary radii of 1.01 and 0.28R_J for planets b and c, respectively, along with a mean mass of 0.54M_J for the former. The equilibrium temperature of planet b is roughly 1150 K. We find an eccentricity consistent with zero for planet b.

We identify a third signal present in the RVs that may be due to a giant planet on a longer-period orbit. Our measurements poorly constrain the semiamplitude of this additional signal, and our baseline is shorter than its apparent period. We cannot conclusively rule out stellar activity as the source of this additional signal; stellar activity indicators are shown in Figure 6. We fit this signal with EXOFASTV2 and find that, if it is of planetary origin, it belongs to a companion planet with an orbital period of 624 days. We cannot well constrain its minimum mass, but find a median value of 0.98M_J. We discuss the possibility and implications of this third planet further in Section 4.

The full list of posteriors is provided in Tables 4 and 5. In Figure 3, we show the raw transit data from TESS and overlay the model light curves for planet b (left panels) and planet c



(a) Spectral energy distribution of TOI-4468 in units of flux, as calculated in our global fit with EXOFASTV2.



(b) Detection limits for TOI-4468 obtained using speckle interferometry at SAI-2.5m telescope. The inset contains the autocorrelation function of the object. North is up, east is to the left.

Figure 2. (a) Spectral energy distribution of TOI-4468. (b) Speckle interferometry detection limits.

Table 3
Priors Used to Initialize the Markov Chain Monte Carlo Fit

Parameter	Description	Prior
[Fe/H]	Metallicity	$\mathcal{N}(0.0, 0.25)$
A_V	*V*-band extinction (mag)	$\mathcal{U}[0, 0.75]$
ϖ	Parallax (mas)	$\mathcal{N}(2.645, 0.0134)$

Note. All priors not listed in this table are set to the EXOFASTV2 defaults, which are uninformative uniform priors (see J. D. Eastman et al. 2019, Table 3).

Table 4
Stellar and Planetary Properties and RV Instrument Characteristics

Parameter	Description	Values		
Fitted Stellar Parameters				
$T_{\rm eff}$	Effective temperature (K)	5170^{+120}_{-110}		
$\log_{10}(g)$	Surface gravity (cgs)	$4.571^{+0.020}_{-0.022}$		
$F_{\rm bol}$	Bolometric flux (cgs)	$8.53^{+0.82}_{-0.64} \times 10^{-11}$		
[Fe/H]	Metallicity (dex)	-0.03 ± 0.16		
ϖ	Parallax (mas)	2.645 ± 0.013		
d	Distance (pc)	378.1 ± 1.9		
Derived Stellar Parameters				
$M_\star$	Mass ($M_\odot$)	$0.805^{+0.042}_{-0.038}$		
$R_\star$	Radius ($R_\odot$)	$0.771^{+0.020}_{-0.018}$		
$L_\star$	Bolometric luminosity ($L_\odot$)	$0.381^{+0.036}_{-0.029}$		
$\rho_\star$	Density (g cm^{-3})	$2.49^{+0.15}_{-0.17}$		
Age	Age (Gyr)	$7.4^{+3.9}_{-3.6}$		
A_V	V-band extinction (mag)	$0.22^{+0.14}_{-0.13}$		
Fitted Planetary Parameters		TOI-4468 b	TOI-4468 c	TOI-4468.03[a]
P	Period (days)	$2.77085931 \pm 0.00000036$	7.013900 ± 0.000020	624^{+53}_{-38}
K	RV semiamplitude (m s^{-1})	$89.4^{+3.9}_{-3.5}$	…	$25.8^{+4.5}_{-46}$
$R_p/R_\star$	Radius of planet in stellar radii	$0.13424^{+0.00062}_{-0.00054}$	$0.0367^{+0.0013}_{-0.0011}$	…
$a/R_\star$	Semimajor axis in stellar radii	$10.03^{+0.20}_{-0.23}$	$18.63^{+0.37}_{-0.43}$	371^{+22}_{-17}
$e\cos(\omega)$	…	$0.015^{+0.024}_{-0.016}$	…	…
$e\sin(\omega)$	…	$0.016^{+0.024}_{-0.017}$	…	…
$m_p \sin(i)$	Minimum mass ($M_\oplus$)	$169.6^{+9.8}_{-8.8}$	…	311^{+49}_{-51}
i	Inclination (deg)	$89.35^{+0.44}_{-0.49}$	$88.95^{+0.66}_{-0.50}$	…
T_C	Observed time of conjunction	$2848.554232^{+0.000077}_{-0.000076}$	$2424.2354^{+0.0025}_{-0.0022}$	3736^{+220}_{-23}
T_{14}	Total transit duration (days)	$0.09743^{+0.00036}_{-0.00033}$	$0.1156^{+0.0030}_{-0.0032}$	
Derived Planetary Parameters		TOI-4468 b	TOI-4468 c	TOI-4468.03
R_p	Radius ($R_\oplus$)	$11.29^{+0.31}_{-0.28}$	$3.09^{+0.14}_{-0.12}$	…
m_p	Mass ($M_\oplus$)	$170.1^{+9.7}_{-8.8}$	$11.1^{+4.0}_{-2.6}$ [b]	…
a	Semimajor axis (au)	$0.03592^{+0.00060}_{-0.00057}$	0.0667 ± 0.0011	$1.332^{+0.079}_{-0.061}$
e	Eccentricity	$0.030^{+0.026}_{-0.020}$	$0.122^{+0.16}_{-0.083}$	…
ω	Argument of periastron (deg)	46^{+45}_{-47}	170^{+120}_{-140}	…
$T_{\rm eq}$	Equilibrium temp (K)	1153^{+26}_{-22}	846^{+19}_{-16}	$189.5^{+6.3}_{-6.4}$
b	Transit impact parameter	$0.111^{+0.084}_{-0.076}$	$0.33^{+0.20}_{-0.21}$	…
ρ_p	Density (cgs)	$0.651^{+0.055}_{-0.053}$	$2.06^{+0.74}_{-0.47}$	…
$\log_{10}(g_p)$	Surface gravity (cgs)	3.117 ± 0.028	$3.05^{+0.13}_{-0.11}$	…
$\langle F \rangle$	Incident flux (10^9 erg s^{-1} cm^{-2})	$0.401^{+0.037}_{-0.030}$	$0.1131^{+0.011}_{-0.0095}$	$0.000292^{+0.000041}_{-0.000037}$
Telescope Parameters		NEID		
$\gamma_{\rm rel}$	Relative RV offset (m s^{-1})	$-19.9^{+2.4}_{-3.0}$		
σ_J	RV jitter (m s^{-1})	$0.0^{+6.2}_{-0.00}$		
σ_J^2	RV jitter variance	-12^{+51}_{-17}		

Notes. Median values and 68% confidence intervals are from EXOFASTV2.
[a] We cannot confirm the planetary nature of this radial velocity signal. We include planetary parameters assuming this scenario for completeness.
[b] We report a mass, density, and surface gravity for planet c based on the mass–radius relation of J. Chen & D. Kipping (2017), though we cannot establish a mass measurement from our measured RVs.

(right panels) derived from our fit with EXOFASTV2, generated with the BATMAN package (L. Kreidberg 2015). In the transit plot for planet b (c), we have removed all data obtained during any transit of planet c (b). In Figure 4, we plot three more transits of planet b and one of planet c, taken from ground-based observatories, that we include in our global fit. In Figure 5, we plot the raw RVs and show the model derived from our EXOFASTV2 fit.

3.2. Statistical Validation of TOI-4468 c

While vetting and observational constraints can rule out many astrophysical false-positive sources, these observational limits often cannot rule out the entire false-positive parameter space. To determine the likelihood that the 7 day signal is from an astrophysical source in the false-positive parameter space, we perform a statistical analysis using the publicly available software TRICERATOPS (S. Giacalone & C. D. Dressing 2020; S. Giacalone et al. 2021), using the available photometry and imaging observations of TOI-4468 as constraints.

TRICERATOPS compares the photometric signal to a suite of astronomical false-positive sources including eclipsing binaries, background binaries, background transiting planets, nearby eclipsing binaries, transiting planets around an unresolved bound companion star, and double periods of each. The software was specifically designed for use with TESS observations, accounting for the light-curve extraction aperture, the nearby stars contained

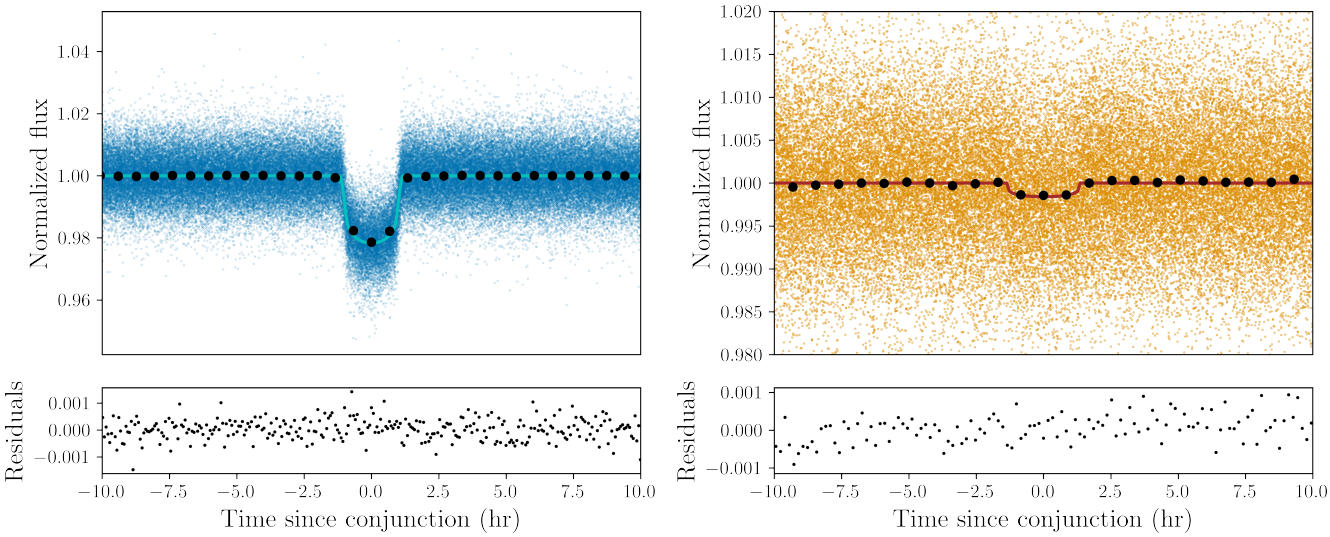


Figure 3. Transit model light curves for both planets, overlaid on the raw photometric measurements taken with TESS. The residuals are binned by a factor of 500. Left: TOI-4468 b. Right: TOI-4468 c.

Table 5
Stellar and Instrumental Photometric Characteristics

Parameter	Description	Values	
Wavelength Parameters		B	R
u_1	Linear limb-darkening coeff.	$0.811^{+0.063}_{-0.066}$	$0.473^{+0.046}_{-0.047}$
u_2	Quadratic limb-darkening coeff.	0.024 ± 0.063	0.202 ± 0.041
		i'	TESS
u_1	Linear limb-darkening coeff.	0.423 ± 0.056	$0.408^{+0.024}_{-0.025}$
u_2	Quadratic limb-darkening coeff.	$0.234^{+0.052}_{-0.051}$	0.214 ± 0.037
Transit Parameters		TESS Full Frame Images	TESS 2 minute cadence
σ^2	Added variance	$3.5^{+1.1}_{-1.0} \times 10^{-7}$	$4.86 \pm 0.27 \times 10^{-6}$
F_0	Baseline flux	0.999952 ± 0.000037	1.000080 ± 0.000029
		SUTO UT 2022-04-09 (B)	RFAC UT 2023-01-11 (R)
σ^2	Added variance	$-2.02^{+0.98}_{-0.72} \times 10^{-5}$	$-3.22^{+0.70}_{-0.52} \times 10^{-5}$
F_0	Baseline flux	$0.99904^{+0.0010}_{-0.00100}$	$0.99890^{+0.00082}_{-0.00081}$
		RFAC UT 2023-04-07 (R)	LCO UT 2024-08-16 (i')
σ^2	Added variance	$-0.0003131^{+0.000011}_{-0.0000090}$	$0.5^{+2.9}_{-2.5} \times 10^{-7}$
F_0	Baseline flux	$0.99978^{+0.00092}_{-0.00090}$	1.00010 ± 0.00014

Note. Median values and 68% confidence intervals are from EXOFASTV2.

within, and all stars within 2.′5 of the target when calculating the false-positive probability (FPP) of the signal and the likelihood that the signal is a false positive originating from a nearby star (the nearby FPP, or NFPP).

To perform the FPP analysis with TRICERATOPS, we used the TESS SPOC PDCSAP 2 minute cadence light curves for all available TESS sectors. Since TRICERATOPS accounts for the TESS extraction aperture in the FPP calculation, we used the PDCSAP apertures provided by the SPOC where applicable. We also incorporated the I-band contrast curve from the SPP instrument and the constraints on potential nearby stars as the source of the signal from multiband photometric follow-up.

The TESS light curves were phase-folded using the values from the global fitting found in Table 4. We ran the FPP calculation with TRICERATOPS 20 times and took the average FPP value. This results in a FPP $= 0.041 \pm 5.32 \times 10^{-4}$ for the 7 day signal. This is just short of the FPP < 0.01 necessary to statistically validate the signal as a planet; however, this does not take into account the fact that there is another planet in the system. Signals in systems with multiple transiting planet candidates are considerably more likely to be genuine transiting exoplanets than those in single-candidate systems (D. W. Latham et al. 2011; J. J. Lissauer et al. 2011; N. M. Guerrero et al. 2021). We are therefore able to apply this "multiplicity boost" to the FPP of the 7 day signal. N. M. Guerrero et al. (2021) quantified the multiplicity boost of candidates discovered by TESS to be 20× for systems containing planets larger than $6R_\oplus$. Applying this boost to our the FPP from TRICERATOPS, we obtain FPP $= 2.05 \times 10^{-3}$, well below the FPP $= 0.01$ threshold necessary for statistical validation. Therefore, we consider TOI-4468 c to be a bona fide planet.

We note that we do not perform a separate statistical validation for the inner, 2.8 day signal since not only was a $>5\sigma$ mass measurement obtained for that planet, but also statistical validation for planets $R_p > 8R_\oplus$ may not be valid due to the overlap in parameter space with brown dwarfs.

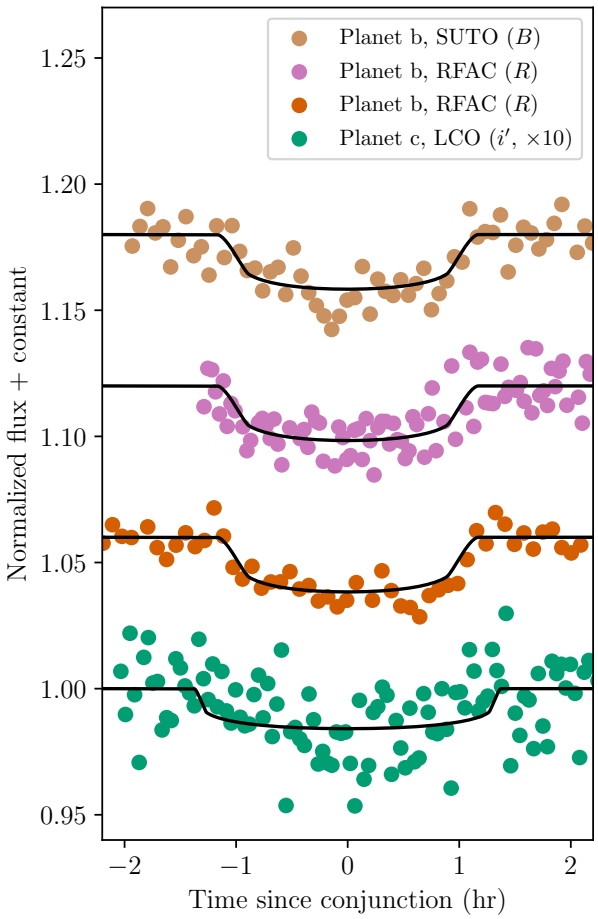


Figure 4. Transit data taken from ground-based observatories. The data from SUTO and RFAC exhibit transits of planet b, while the transit from LCO is of planet c (the difference in normalized flux for this transit is magnified here by a factor of 10 for visibility). These data are included in our global fit with EXOFASTV2.

3.3. Transit Timing Variations

Systems containing HJs and nearby companions have been previously observed to have significant transit timing variations (TTVs; e.g., C. X. Huang et al. 2020) due to planet–planet interactions. These interactions are stronger for planet pairs near a mean motion commensurability. The period ratio between TOI-4468 c and b is roughly 2.53, slightly exterior to the 5:2 commensurability. To test whether this geometry produces observable planet–planet interactions, we perform a one-parameter fit using BATMAN to each individual transit in the 2 minute cadence data, holding all system parameters fixed to the best-fit solution listed in Table 4 and allowing only the midtransit time and continuum shape to vary. Transits lacking at least 2.0 transit durations of data centered on the transit time, as well as transits involving overlapping events from both planets within two durations, were excluded from the fit. This resulted in the exclusion of 11 events for TOI-4468 b and 11 events for TOI-4468 c.

Fits to a flat-line model yield reduced χ^2 values of 2.1 and 1.8 for TOI-4468 b and c, respectively, suggesting either the presence of a small amount of excess timing scatter beyond the formal uncertainties or that our uncertainties are underestimated. To check the possible TTV amplitudes that would be compatible with the data, we compute the weighted rms of the residuals of the $O-C$ values. This yields values of 3.4 minutes for TOI-4468 b and 24.8 minutes for TOI-4468 c, corresponding to 95% upper limits on possible TTV amplitudes of 6.8 minutes and 48.6 minutes, respectively. TTV amplitudes below these thresholds are consistent with the observed transit times, whereas signals exceeding these levels are ruled out by the data.

To examine possible long-term TTV trends in the transit timing signal of TOI-4468 b, we performed an additional fit to the center times of transit computed for the data from each individual TESS sector, using JULIET (N. Espinoza et al. 2019) to fit the period P, center time of transit T_0, $R_p/R_\star$, $a/R_\star$, $\sqrt{e}\cos(\omega)$, and $\sqrt{e}\sin(\omega)$. A single T_0 was computed for each sector of TESS data. The resultant computed T_0 values are consistent to $\sim 1\sigma$, providing no additional evidence of sector-to-sector timing variations.

4. Discussion

4.1. The Possibility of an Inner Companion

TOI-4468 b is to date the only known HJ accompanied by a small outer planet but no inner planet. The only other HJ with an identified outer companion, WASP-47 b, also harbors a small interior planet (J. C. Becker et al. 2015). If this system had an inner companion and formed during the disk phase, it should (for most parameter combinations) reside close enough to the orbital plane of the HJ to transit as well (T. MacLean & J. Becker 2025).

The 2.8 day orbit of planet b sets a narrow limit inside which a potential interior companion could reside. Therefore, the natural first question to address is whether it is possible to place a planet here. We adopt the classic stability criterion due to B. Gladman (1993) that $a - a_b \geqslant 2\sqrt{3}R_H$, where

$$R_H = \frac{a + a_b}{2}\left(\frac{m + m_b}{3M_\star}\right)^{1/3} \quad (1)$$

is the mutual Hill radius of planet b and the hypothetical companion.

In Figure 7, we show the calculated stability limits for an inner planet. The overlaid contours are the $2\sqrt{3}R_H$ criterion of B. Gladman (1993) and the more stringent $10R_H$ criterion derived from numerical simulations of two-planet systems (e.g., A. Obertas et al. 2017). The inner boundary on the allowed region is the Roche limit. The Roche radius is

$$R_R = \left(\frac{2\rho_\star}{\rho}\right)^{1/3} R_\star, \quad (2)$$

where $\rho_\star = 2.48$ g cm^{-3}, based on our fitted values for the stellar mass and radius. The planetary density is calculated assuming a spherical planet with radius related to its mass by the prescription of J. Chen & D. Kipping (2017):

$$R = \begin{cases} R_\oplus (m/M_\oplus)^{0.28}, & m < 2M_\oplus \\ 2^{0.28} R_\oplus (m/2M_\oplus)^{0.59}, & m \geqslant 2M_\oplus. \end{cases} \quad (3)$$

A large swath of parameter space interior to the HJ is amenable to hosting a small planet; we cannot in principle rule out the presence of such a companion.

Using a simplistic scaling argument, we can determine approximately the minimum radius at which a transiting planet would have avoided detection as a function of orbital period. The detection significance S scales to a first-order approximation with $R^2/\sqrt{Pt_{\rm dur}}$, where $t_{\rm dur}$ is the duration of the

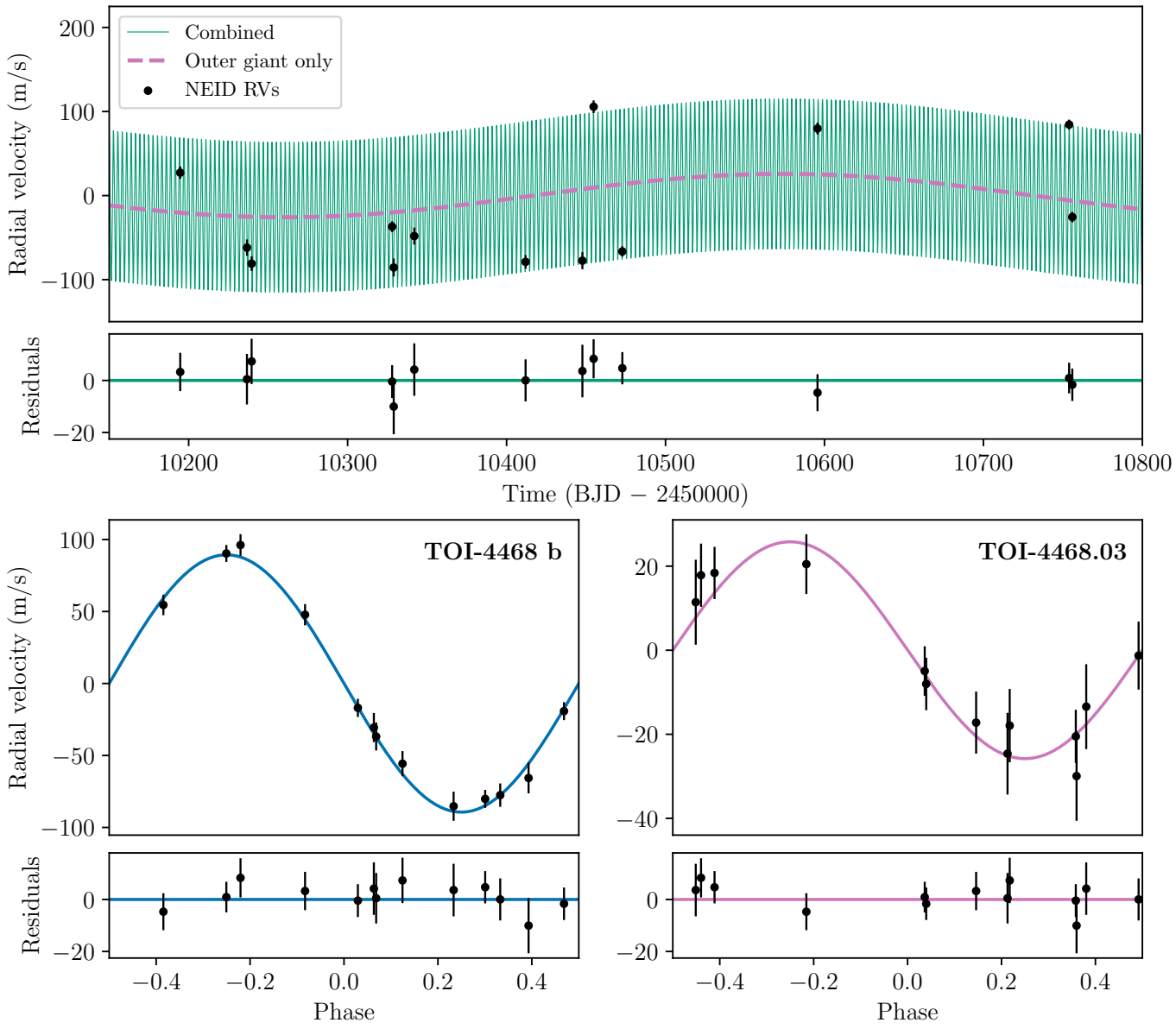


Figure 5. Best-fit RV curves for the giants TOI-4468 b and the unconfirmed TOI-4468.03, both individually and combined. The best-fit eccentricity of planet b is $e_b = 0.030$.

transit (e.g., L. Sha et al. 2026). The transit duration scales with period as $t_{\rm dur} \propto P^{1/3}$ by Kepler's third law. The threshold radius therefore follows

$$R \simeq \left(\frac{P}{P_c}\right)^{1/3}\left(\frac{S}{S_c}\right)^{1/2} R_c. \tag{4}$$

Using the values we report here for the radius and orbital period of planet c, as well as its detection significance ($S_c \sim 25.2\sigma$), we can compute the requisite radius for a 7σ detection at the orbital period of planet b. We find that this radius is roughly $1.2R_\oplus$, indicating that in the stable regime we have identified an undetected inner companion would have a size of at most the order of Earth's.

4.2. The Small Mutual Inclination

A likely cause for the dearth of small outer companions to HJs is the crossing of a secular resonance early in such a system's lifetime (e.g., T. MacLean & J. Becker 2025). This resonance arises when the ratio of two combinations of the secular frequencies is unity (C. Spalding & K. Batygin 2016). Early on, the precession of both planes is primarily due to coupling with the stellar quadrupole, and therefore the star's J_2 controls whether the system is in this resonance. The resonance is swept when

$$J_2 \simeq \frac{1}{6}\frac{m_2}{M_\star}\frac{(\Lambda_1+\Lambda_2)^2}{(\Lambda_1-\Lambda_2)\Lambda_2}\left(\frac{a_1}{R_\star}\right)^2\frac{\alpha^2 b^{(1)}_{3/2}(\alpha)}{1-\alpha^{7/2}}, \tag{5}$$

where $\alpha \equiv a_1/a_2$ and $\Lambda_i \equiv m_i\sqrt{\mathcal{G}M_\star a_i}$ is the circular angular momentum of the ith planet. Here the function

$$b^{(1)}_{3/2}(\alpha) = \frac{2}{\pi}\int_0^\pi \frac{\cos(\psi)\quad d\psi}{[1+\alpha^2-2\alpha\cos(\psi)]^{3/2}} \tag{6}$$

is the usual Laplace coefficient (C. D. Murray & S. F. Dermott 1999). Note that this value changes as the star evolves; in particular, it increases as the star contracts during the pre-main-sequence phase.

Using the values we fit for the system in Section 3, we find that the quadrupole moment necessary to trigger the resonance has varied over the course of the star's life from $J_2 \sim 10^{-3}$–10^{-2}. This range corresponds to an extremely oblate star and is unlikely to have been achieved at any point during the system's history. The time dependence of the stellar J_2 is implicit in the relation

$$J_2 = \frac{1}{3} k_2 \left(\frac{\Omega_\star}{\Omega_b} \right)^2, \tag{7}$$

where k_2 is the star's degree-2 Love number, $\Omega_\star$ is the angular velocity at the surface along its equator, and $\Omega_b = \sqrt{\mathcal{G} M_\star / R_\star^3}$ is the breakup angular velocity. We use the S. P. Matt et al. (2015) model of magnetic braking to compute the spin evolution of the star early in its life. This model applies a time-dependent wind torque to a star whose instantaneous physical state is interpolated from the precomputed evolutionary grids of I. Baraffe et al. (2015). Using the stellar evolution module in the VPLANET code (D. P. Fleming et al. 2019; R. Barnes et al. 2020), we compute $\Omega_\star(t)$ in this way up to an age of 5 Gyr. We also compute the evolution of the stellar radius to get $\Omega_b(t)$. Following J. Becker et al. (2020), we adopt the following simple piecewise continuous evolution for the Love number as the stellar interior transitions from convection dominated to radiation dominated:

$$k_2(t) = \begin{cases} 0.28, & t < 10^7 \,\mathrm{yr} \\ a + bt, & 10^7 \leqslant t \leqslant 10^8 \,\mathrm{yr} \\ 0.014, & t > 10^8 \,\mathrm{yr} \end{cases}. \tag{8}$$

In the above, $a = 0.309566$ and $b = -2.95556 \times 10^{-9}$ yr^{-1}. Having obtained the time dependence of $\Omega_\star$ and k_2, we calculate the evolution of TOI-4468's J_2 over its lifetime. The result is plotted in Figure 8. Clearly, the stellar J_2 never reaches the required value to trigger this resonance.

Because it is unlikely that the system ever encountered the resonance that would evict planet c from the invariable plane, the fact that the mutual inclination between the two planets is small tells us nothing about the stellar obliquity. That this resonance was avoided, however, means that it remains a compelling explanation for the loneliness of HJs, in spite of TOI-4468's coplanarity.

We note also that in the limit where the outer planet is a test particle, even a modest stellar obliquity guarantees a large final mutual inclination between the HJ and its companion, due to the adiabatic change in the phase-space topography as the stellar quadrupole moment decreases (K. Batygin et al. 2016). The planetary mass ratio m_c/m_b in the TOI-4468 system is large enough, however, that the system is better treated by the previously detailed two-massive-planet model of C. Spalding & K. Batygin (2016).

4.3. The Third RV Signal and the Possible Effect of an Outer Giant Planet

There is a clear RV signal with a semiamplitude of 25.8 m s^{-1} and a period of ∼624 days present in our data

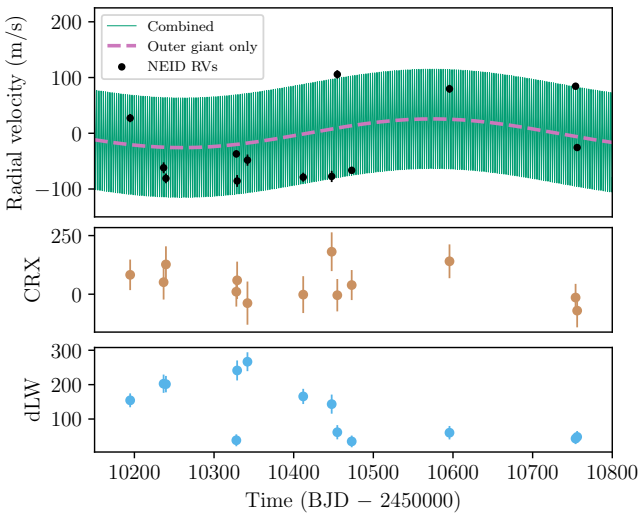


Figure 6. Stellar activity indicators for TOI-4468 measured by NEID: the chromatic index (CRX) and differential line width (dLW). There appears to be some evidence of variation in dLW on the same period as the RV signal attributed to TOI-4468.03. Without more data, however, we cannot verify whether the additional RV signal is due to stellar activity or to a third planet in the system.

(Figure 5, lower-right panel). With the data available to us, we are not able to determine if this signal is due to stellar activity. Stellar activity indicators (Figure 6) show some degree of correlation with the ∼624 day signal, but the quantity of RV data available is insufficient to prove either that the signal is due to stellar activity. For this reason, we must await future RV data, which will allow for a determination of whether TOI-4468.03 is a bona fide planet or not. If this signal is evidence of an additional outer giant in the system, and not stellar activity, then this would raise some new dynamical implications.

The possible presence of a cold Jupiter in the system could contribute an additional quadrupole-order term to the gravitational potential felt by planet c, intruding upon the two-planet resonant picture of inclination evolution developed by C. Spalding & K. Batygin (2016).

D. Lai & B. Pu (2017) show that a distant and massive third body in a three-planet system can dynamically couple the inner two, arresting mutual inclination growth in the inner system. The strength of this coupling is set by the parameter

$$\varepsilon_{bc} \equiv \frac{\nu_{cd} - \nu_{bd}}{\nu_{bc} + \nu_{cb}} \ll 1, \tag{9}$$

which sets the maximum mutual inclination of the inner planets θ_{bc} as a function of the outer giant's inclination. To leading order in θ_{bc},

$$||\sin(\theta_{bc,\max})|| \simeq \varepsilon_{bc} ||\sin(2I_d)||. \tag{10}$$

Because both planets b and c are transiting, the maximum possible value of θ_{bc} is a few degrees, and $\sin(\theta_{bc,\max}) \lesssim 10^{-2}$. The precessional frequencies in Equation (9) are

$$\nu_{bc} = \frac{\mathcal{G} m_b m_c a_b}{4 a_c^2 \Lambda_b} b_{3/2}^{(1)} \left(\frac{a_b}{a_c} \right), \tag{11}$$

$$\nu_{cb} = \frac{\mathcal{G} m_b m_c a_b}{4 a_c^2 \Lambda_c} b_{3/2}^{(1)} \left(\frac{a_b}{a_c} \right), \tag{12}$$

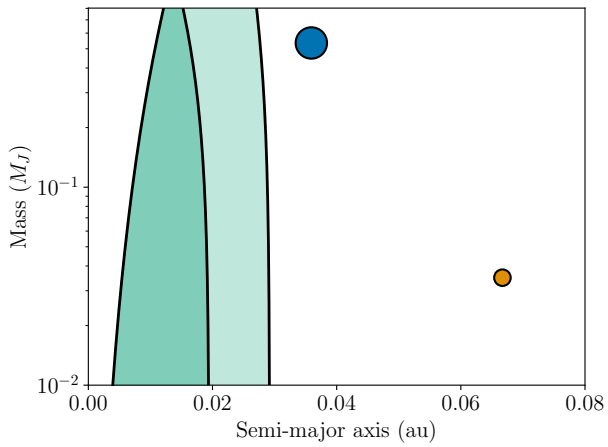


Figure 7. Stability limits for a possible inner companion to TOI-4468 b. The innermost boundary is the Roche limit. The dark green area is the conservatively stable regime (beyond $10R_{\rm H}$ from planet b). The light green area is the Hill-stable regime (beyond $2\sqrt{3}\,R_H$ from planet b). The locations of the two confirmed planets in this parameter space are shown for reference.

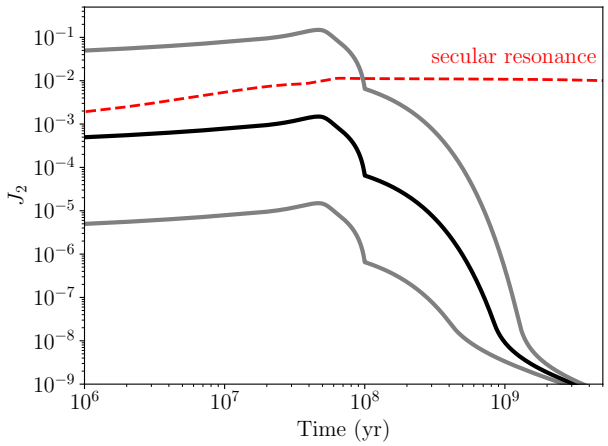


Figure 8. Estimated temporal evolution of TOI-4468's J_2 for a range of initial rotation periods, $0.1 < P_{\rm rot} < 10$ days. The necessary J_2 to achieve a secular resonance between planets b and c is highlighted. The case with an initial rotation period of 1 day is traced by the black curve. J_2 may reach the resonant value for initial rotation periods significantly shorter than 1 day. It is therefore unlikely, but not impossible, that this resonance was ever crossed in the system's history. The kink at 10^8 years is due to k_2 becoming constant as the star's interior becomes fully radiation dominated. At ages >1 Gyr, k_2 and Ω_b are roughly constant, so $J_2 \propto t^{-1}$ per the braking law of A. Skumanich (1972).

$$\nu_{bd} = \frac{3\mathcal{G}m_b m_d a_b^2}{4a_d^3\Lambda_b}, \tag{13}$$

$$\nu_{cd} = \frac{3\mathcal{G}m_b m_d \sqrt{a_b a_c^3}}{4a_d^3\Lambda_b}, \tag{14}$$

where we have expanded the Laplace coefficients pertaining to the outer giant to quadrupole order: $b_{3/2}^{(1)}(\alpha) \simeq 3\alpha$ (e.g., C. D. Murray & S. F. Dermott 1999). Using the median values we have obtained from EXOFASTV2 and an estimated mass of roughly $11M_\oplus$ for planet c from the mass–radius relation of J. Chen & D. Kipping (2017), we obtain $\varepsilon_{bc} \sim 10^{-4}$, indicating that this potential third planet strongly couples the orbits of the inner two regardless of its inclination relative to the inner system's orbital plane. Inclination growth is suppressed by secular torques, therefore, even if the resonant J_2 has been achieved.[26]

We note the analogy to the only other known HJ with a close outer companion: WASP-47. Both planetary systems bear an outer giant of greater mass than the HJ at $P \sim 600$ days. As outlined above, these outer giants may be responsible for coupling the orbits in the inner system and rendering the close companions detectable. If TOI-4468.03 is eventually confirmed as a real planet, the similarity of the TOI-4468 system to the WASP-47 system may allow for additional insights into its likely formation history, including an assessment of whether the two-stage formation process proposed in L. M. Weiss et al. (2017)—in which the giant planets form out of the initial gas-rich protoplanetary disk and are followed by the later in situ formation of the sub-Neptune when the disk is gas-poor—could have operated in the TOI-4468 system.

5. Conclusions

TOI-4468 is a transiting planetary system comprising a hot Jupiter and a lone, mini-Neptune-sized outer companion. Using light curves from TESS and ground-based observatories, together with RV measurements taken with the NEID spectrograph, we have performed a global characterization of this system. Additionally, we have considered the possibility of an additional planet in the system and the consequences of the small mutual inclination between the HJ and its outer companion. We conclude as follows:

1. The TOI-4468 planetary system features a HJ (planet b) on a 2.77 day orbit, with a close outer companion (planet c) on a 7.01 day orbit and no observed inner companion —the only known system with this architecture.
2. TOI-4468 b has a mass of $0.54M_{\rm J}$ and a radius $1.01R_{\rm J}$, from a joint light curve and RV fit. TOI-4468 c has a radius of $0.28R_{\rm J}$, but we do not constrain its mass.
3. We identify an additional RV signal that may be due to an outer giant with a minimum mass of $0.98M_{\rm J}$ on a 624 day orbit. We cannot, however, rule out stellar activity as the source of this signal; more data are needed.
4. We cannot rule out the existence of a planet interior to planet b. However, any undetected planet would need to be $\lesssim R_\oplus$ in size.
5. The resonance mechanism invoked to explain the paucity of outer companions to those HJs that did not undergo high-eccentricity migration may have been thwarted in this system by either of two possible means. Either the stellar J_2 never reached the necessary value to achieve this resonance, or the possible outer giant in the system dynamically coupled their orbits.

Acknowledgments

The corresponding author is grateful to Rich Townsend and Daniel Jontof–Hutter for useful conversations. We thank the authors of J. Schulte et al. (2024, 2025) for making plotting scripts publicly available that informed parts of our

[26] Note that we have adopted here the median minimum mass of the third planet from our EXOFASTV2 fit as m_d, which is very poorly constrained. Because $\varepsilon_{bc} \propto m_d$, this result depends strongly on m_d, but the coupling would be strong for m_d within a few orders of magnitude of M_J.

visualizations. We are grateful to the anonymous reviewer, whose suggested revisions improved the clarity of this manuscript and the reproducibility of our analysis.

J.R.L. is supported by the TESS Guest Investigator program (grant No. 80NSSC25K7901). This work was funded in part by the University of Wisconsin–Madison Research Forward program sponsored by the Office of the Vice Chancellor for Research (OVCR) through funding provided by the Wisconsin Alumni Research Foundation (WARF). B.J.H. is supported by an appointment to the NASA Postdoctoral Program at NASA Goddard Space Flight Center, administered by Oak Ridge Associated Universities under contract with NASA (ORAU-80HQTR21CA005). C.X.H. is supported by ARC Future Fellowship FT240100016. K.A.C. acknowledges support from the TESS mission via subaward s3449 from MIT. I.A.S. acknowledges the support of M. V. Lomonosov Moscow State University Program of Development. The authors acknowledge support from the Swiss NCCR PlanetS and the Swiss National Science Foundation. This work has been carried out within the framework of the NCCR PlanetS, supported by the Swiss National Science Foundation under grant Nos. 51NF40182901 and 51NF40205606. Funding for K.B. was provided by the European Union (ERC AdG SUBSTELLAR, GA 101054354). J.K. acknowledges support from the Swedish Research Council (project grant Nos. 2017-04945 and 2022-04043) and of the Swiss National Science Foundation under grant No. TMSGI2_211697. H.P. acknowledges support by the Spanish Ministry of Science and Innovation with the Ramón y Cajal fellowship number RYC2021-031798-I. Funding from the University of La Laguna and the Spanish Ministry of Universities is acknowledged. A.J. would like to thank the Peter Livingston Scholars Program at the University of Wisconsin–Madison for their generous support. T.M. acknowledges support from the National Science Foundation Graduate Research Fellowship Program (grant No. DGE-2146755).

Based in part on data obtained by the NEID spectrograph, built by Penn State University and operated at the WIYN Observatory by NOIRLab, under the NN-EXPLORE partnership of the National Aeronautics and Space Administration and the National Science Foundation. The NEID archive is operated by the NASA Exoplanet Science Institute at the California Institute of Technology. We thank the NEID Queue Observers and WIYN Observing Associates for their skillful execution of our observations. Based on observations at NSF Kitt Peak National Observatory, NSF NOIRLab, which is managed by the Association of Universities for Research in Astronomy (AURA) under a cooperative agreement with the U.S. National Science Foundation. The authors are honored to be permitted to conduct astronomical research on I'oligam Du'ag (Kitt Peak), a mountain with particular significance to the Tohono O'odham.

This work makes use of observations from the LCOGT network. Part of the LCOGT telescope time was granted by NOIRLab through the Mid-Scale Innovations Program (MSIP). MSIP is funded by NSF.

This research has made use of the Exoplanet Follow-up Observation Program (ExoFOP; doi: 10.26134/ExoFOP5) website, which is operated by the California Institute of Technology, under contract with the National Aeronautics and Space Administration under the Exoplanet Exploration Program.

Funding for the TESS mission is provided by NASA's Science Mission Directorate.

Data Availability

The light-curve data presented in this article were obtained from the Mikulski Archive for Space Telescopes (MAST) at the Space Telescope Science Institute. The specific observations analyzed can be accessed via doi:10.17909/6fdy-r386. The detrended TESS light curves are available on Zenodo (doi:10.5281/zenodo.20029593). Speckle images and light curves from ground-based observatories are available on ExoFOP (NExScI 2022). The processed RV data we collected with NEID are reported in Table 1.

Facilities: TESS, WIYN, LCOGT, RFAC, SUTO.

Software: EXOFASTV2 (J. D. Eastman et al. 2019), TRICERATOPS (S. Giacalone et al. 2021; S. Giacalone & C. D. Dressing 2020), VPLANET (R. Barnes et al. 2020), BATMAN (L. Kreidberg 2015), NUMPY (C. R. Harris et al. 2020), MATPLOTLIB (J. D. Hunter 2007), ASTROPY (Astropy Collaboration et al. 2022), PANDAS (W. McKinney 2010), ASTROIMAGEJ (K. A. Collins et al. 2017), TAPIR (E. Jensen 2013).

ORCID iDs

Joseph R. Livesey https://orcid.org/0000-0003-3888-3753
Benjamin J. Hord https://orcid.org/0000-0001-5084-4269
Juliette Becker https://orcid.org/0000-0002-7733-4522
Andrew Vanderburg https://orcid.org/0000-0001-7246-5438
Joseph E. Rodriguez https://orcid.org/0000-0001-8812-0565
Elise Koo https://orcid.org/0009-0007-0740-0954
Chelsea X. Huang https://orcid.org/0000-0003-0918-7484
Guðmundur Stefánsson https://orcid.org/0000-0001-7409-5688
Karen A. Collins https://orcid.org/0000-0001-6588-9574
Ivan A. Strakhov https://orcid.org/0000-0003-0647-6133
Zijun He https://orcid.org/0009-0009-6918-3259
Maxwell A. Kroft https://orcid.org/0009-0002-2757-4138
Robert Aloisi https://orcid.org/0000-0003-2822-616X
Khalid Barkaoui https://orcid.org/0000-0003-1464-9276
Alyssa Jankowski https://orcid.org/0000-0003-4287-004X
Judith Korth https://orcid.org/0000-0002-0076-6239
Coleman Nelson https://orcid.org/0009-0009-2277-799X
Hannu Parviainen https://orcid.org/0000-0001-5519-1391
Adam Popowicz https://orcid.org/0000-0003-3184-5228
Manfred Raetz https://orcid.org/0000-0002-2190-3319
Richard P. Schwarz https://orcid.org/0000-0001-8227-1020
Eva Stafne https://orcid.org/0009-0001-2913-792X
Keivan G. Stassun https://orcid.org/0000-0002-3481-9052
Thomas G. Beatty https://orcid.org/0000-0002-9539-4203
Thomas MacLean https://orcid.org/0009-0001-6894-2657
Devansh Mathur https://orcid.org/0009-0009-0948-8819
Lizhou Sha https://orcid.org/0000-0001-5401-8079
Melinda Soares-Furtado https://orcid.org/0000-0001-7493-7419

References

Astropy Collaboration, Price-Whelan, A. M., Lim, P. L., et al. 2022, ApJ, 935, 167
Baraffe, I., Homeier, D., Allard, F., & Chabrier, G. 2015, A&A, 577, A42
Barnes, R., Luger, R., Deitrick, R., et al. 2020, PASP, 132, 024502
Batygin, K., Bodenheimer, P. H., & Laughlin, G. P. 2016, ApJ, 829, 114
Becker, J. 2026, ApJ, 997, 327

Becker, J., Batygin, K., Fabrycky, D., et al. 2020, AJ, 160, 254
Becker, J. C., Vanderburg, A., Adams, F. C., Rappaport, S. A., & Schwengeler, H. M. 2015, ApJL, 812, L18
Beleznay, M., & Kunimoto, M. 2022, MNRAS, 516, 75
Boley, A. C., Granados Contreras, A. P., & Gladman, B. 2016, ApJL, 817, L17
Brown, T. M., Baliber, N., Bianco, F. B., et al. 2013, PASP, 125, 1031
Cañas, C. I., Wang, S., Mahadevan, S., et al. 2019, ApJL, 870, L17
Chen, J., & Kipping, D. 2017, ApJ, 834, 17
Collins, K. 2019, AAS Meeting, 233, 140.05
Collins, K. A., Kielkopf, J. F., Stassun, K. G., & Hessman, F. V. 2017, AJ, 153, 77
Dawson, R., & Johnson, J. A. 2018, AR&AA, 787
Eastman, J. D., Rodriguez, J. E., Agol, E., et al. 2019, arXiv:1907.09480
Espinoza, N., Kossakowski, D., & Brahm, R. 2019, MNRAS, 490, 2262
Fleming, D. P., Barnes, R., Davenport, J. R. A., & Luger, R. 2019, ApJ, 881, 88
Gelman, A., & Rubin, D. B. 1992, StaSc, 7, 457
Giacalone, S., & Dressing, C. D. 2020, triceratops: Candidate exoplanet rating tool, Astrophysics Source Code Library, ascl:2002.004
Giacalone, S., Dressing, C. D., Jensen, E. L. N., et al. 2021, AJ, 161, 24
Gladman, B. 1993, Icar, 106, 247
Guerrero, N. M., Seager, S., Huang, C. X., et al. 2021, ApJS, 254, 39
Harris, C. R., Millman, K. J., van der Walt, S. J., et al. 2020, Natur, 585, 357
Hord, B. J., Colón, K. D., Berger, T. A., et al. 2022, AJ, 164, 13
Huang, C. X., Quinn, S. N., Vanderburg, A., et al. 2020, ApJL, 892, L7
Hunter, J. D. 2007, CSE, 9, 90
Jenkins, J. M., Twicken, J. D., McCauliff, S., et al. 2016, SPIE, 9913, 99133E
Jensen, E. 2013, Tapir: A web interface for transit/eclipse observability, Astrophysics Source Code Library, ascl:1306.007
Kanodia, S., Lin, A. S. J., Lubar, E., et al. 2023, AJ, 166, 105
Korth, J., Chaturvedi, P., Parviainen, H., et al. 2024, ApJL, 971, L28
Kreidberg, L. 2015, PASP, 127, 1161
Lai, D., & Pu, B. 2017, AJ, 153, 42
Latham, D. W., Rowe, J. F., Quinn, S. N., et al. 2011, ApJL, 732, L24
Lissauer, J. J., Ragozzine, D., Fabrycky, D. C., et al. 2011, ApJS, 197, 8
MacLean, T., & Becker, J. 2025, ApJ, 987, 30
Matt, S. P., Brun, A. S., Baraffe, I., Bouvier, J., & Chabrier, G. 2015, ApJL, 799, L23
Mayor, M., & Queloz, D. 1995, Natur, 378, 355
McCully, C., Volgenau, N. H., Harbeck, D.-R., et al. 2018, SPIE, 10707, 107070K
McKinney, W. 2010, in Proc. the 9th Python in Science Conf., ed. Stéfan van der Walt & J. Millman (SciPy), 56
Murray, C. D., & Dermott, S. F. 1999, Solar System Dynamics (Cambridge Univ. Press)
Mustill, A. J., Davies, M. B., & Johansen, A. 2015, ApJ, 808, 14
NExScI 2022, Exoplanet Follow-up Observing Program Web Service (IPAC)
Obertas, A., Van Laerhoven, C., & Tamayo, D. 2017, Icar, 293, 52
Olmschenk, G., Ishitani Silva, S., Rau, G., et al. 2021, AJ, 161, 273
Pepper, J., Kane, S. R., Rodriguez, J. E., et al. 2020, AJ, 159, 243
Quinn, S. N., Rodriguez, J. E., Collins, K. A., et al. 2026, AJ, 171, 359
Radzom, B. T., Dong, J., Rice, M., et al. 2025, AJ, 169, 189
Robertson, P., Anderson, T., Stefánsson, G., et al. 2019, JATIS, 5, 015003
Schulte, J., Rodriguez, J. E., Bieryla, A., et al. 2024, AJ, 168, 32
Schulte, J., Rodriguez, J. E., Latham, D. W., et al. 2025, MNRAS, 543, 292
Sha, L., Vanderburg, A. M., Huang, C. X., et al. 2023, MNRAS, 524, 1113
Sha, L., Vanderburg, A. M., Huang, C. X., et al. 2026, AJ, 172, 183
Skumanich, A. 1972, ApJ, 171, 565
Spalding, C., & Batygin, K. 2016, ApJ, 830, 5
Spalding, C., & Batygin, K. 2017, AJ, 154, 93
Stassun, K. G., Oelkers, R. J., Pepper, J., et al. 2018, AJ, 156, 102
Stefánsson, G., Hearty, F., Robertson, P., et al. 2016, ApJ, 833, 175
Stefánsson, G., Mahadevan, S., Petrovich, C., et al. 2022, ApJL, 931, L15
Strakhov, I. A., Safonov, B. S., & Cheryasov, D. V. 2023, AstBu, 78, 234
Vanderburg, A., Huang, C. X., Rodriguez, J. E., et al. 2019, ApJL, 881, L19
Weiss, L. M., Deck, K. M., Sinukoff, E., et al. 2017, AJ, 153, 265
Zechmeister, M., Reiners, A., Amado, P. J., et al. 2018, A&A, 609, A12
Zink, J. K., & Howard, A. W. 2023, ApJL, 956, L29